

1
2
3
4
5
6
7
8
9
10
11
12
13
14
15
16

**Chemical characterization of submicron regional background aerosols in the Western
Mediterranean using an Aerosol Chemical Speciation Monitor**

M.C. Minguillón¹, A. Ripoll^{1,2}, N. Pérez¹, A.S.H. Prévôt³, F. Canonaco³, X. Querol¹, A. Alastuey¹

¹Institute of Environmental Assessment and Water Research (IDAEA-CSIC), Jordi Girona 18-26,
Barcelona, 08034, Spain

²Departament d'Astronomia i Meteorologia, Universitat de Barcelona, Martí i Franquès 1,
08028, Barcelona, Spain

³Paul Scherrer Institute, Laboratory of Atmospheric Chemistry, 5232 Villigen PSI, Switzerland

*Corresponding author: mariacruz.minguillon@idaea.csic.es

17

18 **ABSTRACT**

19 An Aerosol Chemical Speciation Monitor (ACSM, Aerodyne Research Inc.) was
20 deployed at Montseny (MSY, 720 m a.s.l.) regional background site in the Western
21 Mediterranean from June 2012 to July 2013 to measure real-time inorganic (nitrate, sulphate,
22 ammonium and chloride) and organic submicron aerosol concentrations. Co-located
23 measurements were also carried out including real-time submicron particulate matter (PM₁)
24 and black carbon (BC) concentrations, and off-line PM₁ chemical analysis. This is one of the few
25 studies that compare ACSM data with off-line PM₁ measurements, avoiding the tail of the
26 coarse mode included in the PM_{2.5} fraction. The ACSM + BC concentrations agreed with the
27 PM₁ measurements, and strong correlation was found between the concentrations of ACSM
28 species and the off-line measurements, although some discrepancies remain unexplained.
29 Results point to a current underestimation of the relative ionization efficiency (RIE) established
30 for organic aerosol (OA), which should be revised in the future. The OA was the major
31 component of submicron aerosol (53% of PM₁), with a higher contribution in summer (58% of
32 PM₁) than in winter (45% of PM₁). Source apportionment of OA was carried out by applying
33 Positive Matrix Factorization (PMF) using the Multilinear Engine (ME-2) to the organic mass
34 spectral data matrix. Three sources were identified in summer: hydrocarbon-like OA (HOA),
35 low-volatile oxygenated OA (LV-OOA), and semi-volatile oxygenated OA (SV-OOA). The
36 secondary OA (SOA, 4.8 µg m⁻³, sum of LV-OOA and SV-OOA) accounted for 85% of the total
37 OA and its formation during daytime (mainly SV-OOA) was estimated to be 1.1 µg m⁻³. In
38 winter, HOA was also identified (12% of OA), a contribution from biomass burning OA was
39 included, and it was not possible to differentiate two different SOA factors but a single OOA
40 factor was resolved. The OOA contribution represented the 60% of the total OA, with a degree
41 of oxidation higher than both OOA summer factors. An intense wildfire episode was studied
42 obtaining a region-specific BBOA profile.

43

44 **KEYWORDS:** ACSM, PM₁, organics, chemical composition, Mediterranean, air quality.

45

46 **1 INTRODUCTION**

47 Ambient aerosols have adverse effects on human health (Pope III and Dockery, 2006),
48 and affect climate (IPCC, 2013), ecosystems, crops, and regional visibility. Fine particulate
49 matter (PM₁, particles with an aerodynamic diameter <1 µm) contains substantial fractions of
50 inorganic compounds and carbonaceous aerosols, the latter reaching up to 90% of the mass
51 (Jimenez et al., 2009). Carbonaceous aerosols are comprised of organic compounds,
52 collectively referred to as organic aerosol (OA), elemental carbon (EC), and carbonates (from
53 mineral dust), although the latter can be considered negligible in submicron aerosols.

54 The Western Mediterranean Basin (WMB) has special atmospheric and geographic
55 characteristics that imply the interest of the detailed study of the ambient aerosols in this area
56 (Querol et al., 2009). The regional background has been investigated through long data series
57 of measurements in previous studies available at Montseny (representative of the regional
58 background in the WMB). Pérez et al. (2008) found average particulate matter concentrations
59 at Montseny of 17, 13 and 11 µg m⁻³ of PM₁₀, PM_{2.5} and PM₁, respectively, in the 2002-2007
60 period. Cusack et al. (2012) and Querol et al. (2014) found a decreasing trend in PM_{2.5}
61 concentrations from 2001 to 2012 of -0.39 µg m⁻³ per year. PM_{2.5} concentrations were found
62 higher in the WMB than at other rural background sites across Spain, Portugal, Germany and
63 Scandinavia but lower than those measured in Switzerland, Italy and Austria (Cusack et al.,
64 2012). The prevailing daily evolution is driven by the breeze circulation (mountain and sea
65 breezes), with lower PM_x concentrations at night owing to the nocturnal drainage flows, and
66 higher PM_x concentrations at midday owing to the transport of atmospheric pollutants
67 accumulated in the pre-coastal depression upwards by the breeze (Pérez et al., 2008).
68 Maximum PM₁₀ concentrations were found in summer, February-March and November, and
69 sporadic PM_x increases may be recorded under anticyclonic conditions (Pey et al., 2010). The
70 chemical composition of PM_{2.5} is characterised by high concentrations of organic aerosol and
71 sulphate, followed by crustal material, nitrate and ammonia, with sea spray and elemental
72 carbon being a minor part of the total PM_{2.5} mass (Cusack et al., 2012). Compared to other
73 central European sites, the Western Mediterranean aerosol is characterised by higher
74 concentrations of crustal material but lower concentrations of organic aerosol, elemental
75 carbon and ammonium nitrate (Pey et al., 2009). Nevertheless, relatively high PM_{2.5}
76 concentrations of carbonaceous aerosol and sulphate transported from populated coastal
77 areas are regularly recorded, especially during winter anticyclonic episodes and summer
78 midday PM highs (Pey et al., 2009;Pey et al., 2010). A organic carbon (OC) to elemental carbon
79 (EC) ratio (14 in summer, 10 in winter) was detected, pointing to the influence of biogenic

80 emissions, secondary organic aerosol (SOA) formation favoured by high ozone concentrations
81 and insolation, and intensive recirculation of aged air masses (Pey et al., 2009;Querol et al.,
82 2013).

83 The sources of organic aerosol in the regional background site of Montseny were
84 studied in two intensive campaigns, using off-line ¹⁴C analysis (Minguillón et al., 2011), Aerosol
85 Mass Spectrometers (AMS) (Minguillón et al., 2011;Crippa et al., 2014), and organic tracers
86 (Alves et al., 2012;Van Drooge et al., 2012). Minguillón et al. (2011) found that the contribution
87 of fossil fuel combustion sources (mainly road traffic emissions) to OC at Montseny was 31%
88 and 25%, in winter and summer, respectively, and that 85% of this fossil OC was secondary.
89 The contribution of biomass burning emissions was relatively low when compared with other
90 regional background sites in Europe, and was estimated to be 21% and 12% of the total OC in
91 winter and summer, respectively. Alves et al. (2012) concluded that the anthropogenic input
92 may be associated with the transport of aged air masses from the surrounding industrial/urban
93 areas, which superimpose the locally originated biogenic hydrocarbons.

94 Besides these studies, a long time series of organic aerosol data has not been analysed
95 in Montseny. To this end, the newly-developed Aerosol Chemical Speciation Monitor (ACSM)
96 would be suitable (Ng et al., 2011b), as opposed to the use of AMS, which cannot work
97 unattended and therefore is usually employed around the world for periods of about one
98 month. Nevertheless, due to its recent implementation, some studies based on ACSM data are
99 found in the literature (Ng et al., 2011b;Shaw et al., 2012;Sun et al., 2012;Budisulistiorini et al.,
100 2013;Canonaco et al., 2013;Carbone et al., 2013;Sun et al., 2013a;Sun et al., 2013b;Takahama
101 et al., 2013;Bougiatioti et al., 2014;Canonaco et al., 2014;Petit et al., 2014;Ripoll et al., 2014a).

102 The present study aims at interpreting a one-year time series of inorganic and organic
103 compounds in the submicron aerosol in the regional WMB, with special focus on their
104 evolution throughout the year as a function of the concatenation of different atmospheric
105 scenarios. The different types and origin of organic aerosol (OA) are also investigated. To this
106 end, an ACSM was deployed for a year in the regional background site of Montseny (MSY),
107 according to the schedule planned within the Aerosols, Clouds, and Trace gases Research
108 InfraStructure (ACTRIS) Network project. Moreover, a validation of the ACSM data is carried
109 out by comparison with co-located instruments both real-time and off-line.

110

111 **2 METHODOLOGY**

112 **2.1 Sampling site**

113 The MSY station (41°46'46"N, 02°21'29"E, 720 m a.s.l.) is located in the Montseny
114 natural park, in a densely forested area, 50 km to the N-NE of the Barcelona urban area, and
115 25 km from the Mediterranean coast. The station is located on the upper walls of a valley
116 extending perpendicularly from the Catalan Pre-Coastal ranges to the coast. The site is
117 relatively far from urban and industrial areas, but it can be affected by anthropogenic
118 emissions transported from populated and industrialised areas under specific meteorological
119 conditions. The MSY station is in the ACTRIS Network (formerly EUSAAR, European Supersites
120 for Atmospheric Aerosol Research), is a Global Atmosphere Watch (GAW) site, and is part of
121 the IDAEA-CSIC and the Department of Environment of the Autonomous Government of
122 Catalonia air quality monitoring network.

123 The prevailing atmospheric dynamics has been described elsewhere (Pérez et al.,
124 2008;Pey et al., 2009). Briefly, in winter the location of the Azores high pressure system
125 favours the entry of clean Atlantic air masses into the WMB which replace the existing air
126 masses leading to a decrease of pollutants. In summer, the very weak pressure gradients result
127 in local circulations dominating the atmospheric dynamics with the consequent accumulation
128 of pollutants (Millán et al., 1997). The climate is typical Mediterranean with warm summers,
129 temperate winters and irregular precipitation rates during the year.

130 The daily classification of meteorological episodes affecting MSY during the study
131 period was made as described in Pérez et al. (2008), leading to the following types of scenario:
132 Atlantic Advection, North African, Mediterranean, European, Regional, and Winter Anticyclonic
133 Episodes. The frequency of each type of scenario for each of the months of the study period is
134 shown in [Figure S1](#).

Eliminado: Figure S1

136 **2.2 ACSM settings, calibrations and data processing**

137 An ACSM was deployed from June 2012 to July 2013, according to the ACTRIS
138 schedule, to measure non-refractory submicron aerosol species (organics, nitrate, sulphate,
139 ammonium and chloride) in real-time (Ng et al., 2011b). Briefly, the instrument uses an
140 aerodynamic lens to sample and focus submicron particles (75-650 nm) into a narrow particle
141 beam (Liu et al., 2007), with a flow of approximately 85 cc/min. The beam is transmitted into
142 the final of three vacuum chambers, where particulate matter is flash-vaporized on a hot oven
143 (600 °C), ionized by hard electron impact ionization (70eV) and subsequently detected using a

145 commercial quadrupole mass spectrometer. The concentration of the aforementioned species
146 is calculated based on the measured aerosol mass spectra. For a given species, its
147 concentration is calculated based on the addition of the ion signals at each of its mass spectral
148 fragments and its ionization efficiency (IE) (Canagaratna et al., 2007). Since calibration of IEs
149 for all ambient species is not feasible, the relative ionization efficiency (RIE) (compared to that
150 of nitrate) is used for different species.

151 Thus, mass calibration of the ACSM is based on determining the instrument response
152 factor (RF) using ammonium nitrate calibration aerosol (Ng et al., 2011b). In this study, an
153 atomizer (TSI, Constant Output Atomizer Model 3076) was used for primary aerosol
154 generation, followed by a silica gel diffusion dryer, an SMPS system (model TSI 3936),
155 comprised of an electrostatic classifier (model TSI 3080) with a differential mobility analyzer
156 (DMA, model TSI 3081) and a condensation particle counter (CPC, TSI 3772). Monodisperse
157 300 nm ammonium nitrate aerosol particles were generated for the calibration. The calibration
158 comprised a range of nitrate concentrations from 0 to 15 $\mu\text{g m}^{-3}$, which were achieved by
159 diluting the generated aerosol. RIE for ammonium was directly determined from the
160 ammonium nitrate calibration.

161 Several calibrations were carried out through the sampling period, and average values
162 for nitrate IE and RIE for ammonium were used for the whole dataset. After several tests
163 around the world, more experience has been gained regarding the performance of the ACSM.
164 Hence, RIE for sulphate has been shown to vary from instrument to instrument and therefore
165 the default value (1.2) (Ng et al., 2011b) cannot be directly used. Nevertheless, this
166 information was known when our ACSM was no longer at the MSY station, and hence,
167 sulphate RIE was determined by doing the aforementioned calibration exercise with
168 ammonium sulphate monodisperse aerosol in Barcelona. The sulphate RIE value found was
169 very close to the default value and hence 1.2 was used for the current dataset. The default RIE
170 for organics (1.4) (Ng et al., 2011b) has been used, although some discussion about this can be
171 found in section 3.1.

172 The ACSM was connected to a general inlet equipped with a nafion drier to maintain
173 the RH below 40%, although technical problems resulted in some periods (about 50% of the
174 data points) with uncontrolled RH. The ACSM was set to measure with a time resolution of
175 approximately 30 minutes, resulting from setting it to work with 24 scans (alternatively 1
176 sample and 1 filtered) per data point with a scan speed of 500 ms/amu. The data acquisition
177 software provided by Aerodyne Research (version 1.4.2.5 from the beginning to 18th December
178 2012, and version 1.4.3.8 for the rest of the period) was used to process the measurements.
179 The data were analyzed with the ACSM data analysis software version 1.5.3.2 (Aerodyne

180 Research Inc.) written in Igor Pro (WaveMetrics, Inc., Lake Oswego, OR, USA). A correction for
181 the instrument performance limitations was applied to the dataset based on the inlet pressure
182 and N₂ signal. The aerosol mass concentrations were then corrected for particle collection
183 efficiency (CE) following the Middlebrook approach (Middlebrook et al., 2012). The aerosols at
184 MSY are assumed to be internally mixed and thus the CE was assumed to be the same for
185 different components in contrast to e.g. Hawkins et al. (2010).

186

187 **2.3 Additional measurements and instrumentation**

188 Submicron particulate matter (PM₁) 24-h samples were collected on quartz fibre filters
189 (Pallflex 2500QAT-UP) using DIGITEL (DH-80) high volume (30 m³ h⁻¹) samplers with a PM₁
190 impactor inlet. The sampler, and therefore the collected samples, was kept inside a container
191 with controlled temperature (between 24 and 26°C). Samples were collected every 4 days.
192 Gravimetric PM₁ determination was carried out by weighing the filters before and after
193 sampling, after stabilization in a conditioned room (20°C and 50% relative humidity). Chemical
194 off-line analyses were carried out. A quarter of the filter was acid digested (HNO₃:HF:HClO₄),
195 and the resulting solution was analysed by Inductively Coupled Plasma Atomic Emission
196 Spectroscopy (ICP-AES) for major elements determination, including S, from which the
197 sulphate concentration was calculated. Another quarter of the filter was water extracted to
198 determine the nitrate, sulphate and chloride concentrations by Ion Chromatography and the
199 ammonium concentrations by an ion selective electrode. OC concentrations were determined
200 by thermal-optical methods using a Sunset instrument following the EUSAAR2 thermal
201 protocol (Cavalli et al., 2010). Blank filters were analysed together with the samples and
202 concentrations were subtracted from those found in the samples in order to calculate the
203 ambient concentrations.

204 PM₁ hourly concentrations were measured using an optical particle counter (GRIMM,
205 model 180) and corrected with the simultaneous 24-h gravimetric measurements (Alastuey et
206 al., 2011). Equivalent Black Carbon (BC) mass concentrations (Petzold et al., 2013) were
207 measured with a 1-minute time resolution by a multi-angle absorption photometer (MAAP,
208 model 5012, Thermo) using a PM₁₀ inlet, and using the default mass absorption cross section
209 (MAC) from the instrument software (6.6 m² g⁻¹). Particle number size distributions (9-820 nm)
210 were measured by a Scanning Mobility Particle Sizer (SMPS), comprising a DMA connected to a
211 CPC (TSI 3772), with a system designed and manufactured at the Leibniz Institute for
212 Tropospheric Research (Wiedensohler et al., 2012). The mass concentration from SMPS data

213 was calculated from the total volume of particles and the composition-dependent density
214 calculated based on the ACSM chemical composition.

215 Wind direction and speed, solar radiation, temperature, relative humidity and
216 precipitation were recorded using conventional instruments and hourly data can be seen in

217 [Figure S2](#),

Eliminado: Figure S2

218

219 2.4 Source apportionment of OA

220 The source apportionment to the organic fraction can be investigated by applying
221 Positive Matrix Factorization (PMF) (Paatero and Tapper, 1994) using the Multilinear Engine
222 (ME-2) (Paatero, 1999) to the organic mass spectra. Both methods describe the measurements
223 with a bilinear factor model:

$$224 \quad x_{ij} = \sum_{k=1}^p g_{ik} f_{kj} + e_{ij} \quad (1)$$

225 where x_{ij} is the j^{th} species (m/z) concentration measured in the i^{th} sample, p is the
226 number of sources, g_{ik} is the contribution of the k^{th} source to the i^{th} sample, f_{kj} is the
227 concentration of the j^{th} species in the k^{th} source (mass spectra) and e_{ij} is the residual associated
228 with the j^{th} species concentration measured in the i^{th} sample. The values g_{ik} and f_{kj} are adjusted
229 until a minimum for the objective function Q for a given number of factors p is found:

$$230 \quad Q = \sum_{i=1}^n \sum_{j=1}^m \left(\frac{e_{ij}}{\sigma_{ij}} \right)^2 \quad (2)$$

231 where σ_{ij} is the user defined uncertainty for the j^{th} species in the i^{th} sample.

232 With the ME-2, the user can introduce a priori information about sources e.g. using the
233 so-called a-value approach. Hence, the user inputs one or more factor profiles and a constraint
234 defined by the a-value, which determines the extent to which the output profile can differ
235 from the profile fed to the model.

236 In the present study the source apportionment to OA was performed applying ME-2
237 using the toolkit SoFi (Source Finder) version 4.7 described in Canonaco et al. (2013). The ME-2
238 was applied separately for the warm and cold periods in this study, given the expected
239 differences among them. The warm period was defined as a period with >70% of the days with
240 average $T > 19^{\circ}\text{C}$, hourly max $T > 24^{\circ}\text{C}$ and hourly min $T > 15^{\circ}\text{C}$, which includes 14th June to 9th
241 October 2012. The cold period was defined as a period with >70% of the days with average
242 $T < 10^{\circ}\text{C}$, hourly max $T < 13^{\circ}\text{C}$ and hourly min $T < 8^{\circ}\text{C}$ and includes 28th October 2012 to 7th April
243 2013. Only $m/z \leq 100$ were used for several reasons: a) the signals of $m/z > 100$ account for a

245 minor fraction of the total signal (2% on average), b) the $m/z > 100$ have larger uncertainties,
246 and c) the large interference of naphthalene signals (at m/z 127, 128, and 129) is avoided. The
247 error matrix was calculated by the aforementioned customized software, which downweights
248 the m/z masses calculated from the m/z 44 signal. Moreover, m/z with signal to noise ratio
249 (S/N) below 0.2 were downweighted by a factor of 10, and those with S/N between 0.2 and 1
250 were downweighted by a factor of 2.

251

252 3 RESULTS AND DISCUSSION

253 3.1 Comparison of ACSM data with other measurements

254 This is one of the few studies, together with Ripoll et al. (2014a), that compare ACSM
255 data with off-line PM_{10} measurements. Most of the studies found in the literature comparing
256 ACSM data with off-line measurements are based in the $PM_{2.5}$ fraction for the off-line
257 measurements. In this study we use PM_{10} measurements, avoiding the tail of the coarse mode
258 that the $PM_{2.5}$ fraction includes, and hence being closer to the size range measured by the
259 ACSM (75-650nm).

260 The sum of the ACSM components concentrations and the BC concentrations
261 measured by the MAAP was compared with PM_{10} concentrations determined by the optical
262 particle counter, resulting in a strong correlation (squared Pearson correlation coefficient,
263 $R^2=0.66$) and a slope very close to unity (1.005) (Figure 1). The application of a time-dependent
264 collection efficiency (CE) to the ACSM data based on the Middelbrook approach (Middlebrook
265 et al., 2012) resulted in a better fit compared to the use of a constant $CE=0.5$ used in several
266 studies (which resulted in a slope of 0.913 and a $R^2=0.65$). Hence the time-dependent CE
267 application is considered more suitable for the present study. The time-dependent CE equalled
268 the default value of 0.45 for most of the period, and increased up to 0.65 during the colder
269 period (Figure S3). The sum of ACSM components and BC concentrations was also compared to
270 the mass concentration calculated from SMPS data, resulting in a strong correlation (squared
271 Pearson correlation coefficient, $R^2=0.77$) and a slope very close to unity (0.997) (Figure S4).
272 Moreover, ACSM components concentrations were daily averaged and compared to off-line
273 measurements from 24-h PM_{10} samples (Figure 2). All the species, except for chloride, showed
274 strong correlations (R^2 of 0.68, 0.82 and 0.94 for ammonium, nitrate and sulphate,
275 respectively). Chloride concentrations were below or close to detection limits for both ACSM
276 and off-line analysis, which may be the cause for the discrepancies found. Such discrepancies
277 were also found in other studies (Budisulistiorini et al., 2014). For the strongly-correlated

Eliminado: Figure 1

Eliminado: Figure S3

Eliminado: Figure S4

Eliminado: Figure 2

282 species, the slopes (ACSM vs off-line measurements) were different for each of them. Whereas
283 it was close to unity for sulphate (1.15), it was higher for ammonium (1.72), and much higher
284 for nitrate (2.80). The final reasons for this discrepancy remain unexplained, although a
285 possible cause is the volatilization of ammonium nitrate from the filters. Nevertheless, the
286 volatilization of ammonium nitrate is expected to be low given that the samples are kept at
287 controlled conditions (24-26°C) as described in the methods section. Moreover, if random
288 volatilization occurred, the correlation coefficients found between ACSM and filters would be
289 lower. The apparent discrepancy between the slope for total PM₁ (ACSM+BC vs PM₁ from OPC
290 corrected with gravimetric measurements, close to unity) and the slopes for the different
291 components (>1) is attributed to the undetermined fraction of PM₁ mass in the filters. Thus,
292 whereas the ACSM+BC concentrations are strictly the sum of the components, the PM₁
293 gravimetric concentrations include a fraction of undetermined mass, partially attributed to
294 water (Figure S5).

295 For organic aerosol a strong correlation was found ($R^2=0.82$), and the high slope
296 obtained (4.25) may be interpreted as the OM-to-OC ratio, since the ACSM measures OA and
297 the off-line measurements determined OC. This large OM-to-OC ratio suggests
298 photochemically well-aged organics, but it is too high even for a pure SOA (Aiken et al., 2008),
299 which is expected to have an important contribution at MSY as will be discussed later (section
300 3.5), and it is higher than the OM-to-OC ratio determined in March 2009 at Montseny (2.0)
301 (Minguillón et al., 2011). This extremely large OM-to-OC ratio might be attributed to a)
302 underestimation of OC due to loss of semi-volatile organic compounds from the filters, and b)
303 overestimation of OM by the ACSM due to an underestimation of the RIE for organics. The first
304 reason is expected to be less likely given the strong correlation found between OA and OC
305 (which would not be so if random volatilization occurred) and given that the samples are kept
306 at controlled conditions, as formerly explained, hence reducing the possible volatilization.
307 Previous studies also found higher than expected OM-to-OC ratios when comparing ACSM OA
308 with off-line OC measurements. Budisulistiorini et al. (2014) found OM-to-OC ratios of 4.85
309 and 3.85 in summer and fall, respectively. Ripoll et al. (2014a) found an OM-to-OC ratio of 3.39
310 for a one year sampling period. This topic is currently being investigated by the ACSM
311 manufacturer. The calculation of OM-to-OC ratio from the f44 based on Aiken et al. (2008) was
312 not carried out given that it is not suitable for ACSM instruments, as recently learnt from an
313 intercomparison of 13 Q-ACSM instruments (Fröhlich et al., 2015).

314

Eliminado: Figure S5

316 **3.2 Time series and average composition of submicron aerosol. Seasonal variation**

317 The average concentration (P25, P75) of the ACSM components plus BC concentrations
318 during the study period was $7.3 \mu\text{g m}^{-3}$ (3.1, 10.2). The highest concentrations were measured
319 during the warm periods (average $10.3 \mu\text{g m}^{-3}$), defined as the periods with most of the days
320 with average $T > 20^\circ\text{C}$ (from 14th June to 9th October 2012 and from 13th June to 9th July 2013).
321 The lowest concentrations were recorded during the cold period (average $5.8 \mu\text{g m}^{-3}$), which
322 includes a period with most of the days with average $T < 13^\circ\text{C}$ (from 28th October 2012 to 7th
323 April 2013) (Figure 3). The average monthly concentrations, following the described variation,
324 can be seen in Figure 4. This is in agreement with the seasonal variations observed during a
325 long time period (2002-2010) by Cusack et al. (2012). The summer increase is associated with
326 the recirculation of air masses that prevent air renovation, the low precipitation (Figure S2),
327 and the formation of secondary aerosols enhanced by the maximum solar radiation (Figure
328 S2). The lower winter concentrations can be explained by the high frequency of Atlantic
329 advectons (Figure S1) and the higher precipitation rates, although occasional high
330 concentrations are attributed to winter anticyclonic scenarios (Pey et al., 2010). The seasonal
331 variation of PM_{10} concentrations at MSY is also influenced by the evolution of the boundary
332 layer height, which is lower during wintertime and increases during summertime, especially
333 during the central hours of the day. Changes in the origin of air masses also determined the
334 seasonal variation of PM_{10} concentrations.

335 On average, the most abundant component was OA ($3.8 \mu\text{g m}^{-3}$), followed, in this
336 order, by sulphate ($1.3 \mu\text{g m}^{-3}$), ammonium ($0.8 \mu\text{g m}^{-3}$), nitrate ($0.8 \mu\text{g m}^{-3}$), BC ($0.4 \mu\text{g m}^{-3}$)
337 and chloride ($< 0.1 \mu\text{g m}^{-3}$). The OA contribution varied throughout the year, reaching 60% of
338 the total PM_{10} in the summer period (June, July and August) and decreasing progressively down
339 to 43% in February (Figure 4). The contribution of sulphate followed the same seasonal
340 variation, from about 20% in the warmer months to about 8% in the colder months. The
341 nitrate contribution showed an inverse trend, with higher relative contributions in the winter
342 and much lower in summer. These seasonal variations were already observed in previous
343 studies using off-line filter sampling (Pey et al., 2009; Ripoll et al., 2014b) and can be attributed
344 to a higher SOA contribution, favoured formation of sulphate, and nitrate gas/aerosol
345 partitioning leading to vaporization of ammonium nitrate during the warmer period.

346 When investigating the diurnal patterns, it is observed that OA, nitrate and BC
347 concentrations reach the maximum at around 14h UTC in summer, whereas sulphate and
348 ammonium show a delayed increase in their concentrations, peaking at around 16h UTC
349 (Figure 5). The reasons for this shift may obey to the different origin of each component.

Eliminado: Figure 3

Eliminado: Figure 4

Eliminado: Figure S2

Eliminado: Figure S2

Eliminado: Figure S1

Eliminado: Figure 4

Eliminado: Figure 5

357 Whereas the OA, nitrate and BC are transported with the breeze from the populated areas and
358 the valley towards the regional background site, the sulphate can also be transported from
359 further away, i.e. from over the Mediterranean Sea due to shipping emissions. Later in the day,
360 when the breeze is developed in the opposite direction (from inland towards the coast), the
361 concentrations of OA, BC and nitrate decrease, whereas the sulphate and ammonium
362 concentrations remained high for longer time (until about 19h UTC). This is due to the more
363 regional character of ammonium sulphate, which is present in a wider area due to its longer
364 lifetime in the atmosphere (Seinfeld and Pandis, 2006) and hence remains longer at MSY. In
365 addition to the transport of pollutants, local SOA can be formed (see section 3.5 for
366 discussion). Specific episodes may differ from this average behaviour owing to specific
367 atmospheric characteristics, for which sulphate concentrations increase simultaneously with
368 OA, but the most common variation is the one described here. On the other hand, in winter, all
369 the components show an increase at around 15h UTC, and concentrations remain high until
370 around 22h UTC, when they start to decrease to reach a minimum around 9h UTC (Figure 5).
371 This simultaneous variation indicates that the pollutants are transported from the nearby
372 polluted areas to MSY with the breeze.

Eliminado: Figure 5

374 3.3 Influence of the type of scenario on submicron aerosol

375 The total PM₁ concentrations were investigated as a function of the type of scenario,
376 finding the lowest concentrations during Mediterranean episodes and Atlantic advections, and
377 the highest during North African outbreaks, European episodes and Winter Anticyclonic
378 episodes (Figure 6). Some differences in the relative chemical composition as a function of the
379 type of scenario were found (Figure 6). OA and sulphate relative contributions were higher
380 under regional and North African episodes. This may be due to the higher formation of
381 secondary aerosols enhanced by the higher temperature and solar radiation during these
382 episodes. See additional discussion about formation of SOA in section 3.5. Moreover, the
383 higher sulphate concentrations under regional episodes may also be due to the enhanced
384 regional mixing, as shown by the flatter diurnal pattern shown for this pollutant (Figure S6).
385 Sulphate relative contribution was also high when Mediterranean air masses affected MSY
386 probably owing to the impact of shipping emissions. On the other hand, nitrate relative
387 contribution was found to be higher for Winter Anticyclonic and European episodes. For both
388 cases the colder weather compared to the rest of the year is partly responsible for the higher
389 nitrate concentrations. During Winter Anticyclonic episodes, the stagnant conditions favouring
390 the accumulation of polluted air masses that are transported from the Barcelona metropolitan

Eliminado: Figure 6

Eliminado: Figure 6

Eliminado: Figure S6

395 area towards MSY may also be responsible for the high nitrate concentrations (Pey et al.,
396 2010). Note that this transport takes place later in the day than in warm conditions, thus
397 reaching the maximum concentrations between 15h UTC and 22h UTC, and that the day-night
398 difference is much higher than for other scenarios (Figure S6). During European episodes, the
399 higher nitrate concentration can be attributed to the long range transport of nitrate from
400 Europe to the study area, although this type of episodes often take place under anticyclonic
401 conditions and hence the nitrate may have a local origin at lower heights, whereas European
402 nitrate is transported at higher altitudes, as it was seen by Ripoll et al. (2014b).

Eliminado: Figure S6

403 The relative chemical composition as a function of the total concentration was also
404 investigated, but no clear patterns were identified, meaning that there is not a prevalent
405 component for low or for high concentrations (Figure S7).

Eliminado: Figure S7

407 3.4 Wildfire episode

408 A wildfire episode took place from 22 to 26 July 2012 (Figure 7) at 100 km to the NE of
409 MSY, affecting a wide area (Figure S8). It resulted in an average ACSM components + BC
410 concentrations of $16.5 \mu\text{g m}^{-3}$ over the five-days period. Mainly, the components whose
411 concentrations increased significantly were OA, nitrate and BC, reaching 30-min values of 50
412 $\mu\text{g m}^{-3}$, $4.5 \mu\text{g m}^{-3}$ and $3.6 \mu\text{g m}^{-3}$, respectively, which are 9, 8 and 7 times higher than their
413 respective summer averages. The average relative concentration during this episode was
414 dominated by OA (73%).

Eliminado: Figure 7

Eliminado: Figure S8

415 In order to investigate the wildfire source, an unconstrained source apportionment
416 (PMF) of the organic aerosol fraction during this episode was carried out. The PMF resulted in
417 two factors, one representing the fresh biomass burning organic aerosol (named as
418 BBOA_MSY) and another one interpreted as the mix of other OA sources and aged BBOA,
419 named as OOAm (where the m stands for mix). The interpretation of the factors is based on
420 their mass spectral source profiles and the time series of their contributions. The BBOA_MSY
421 shows higher peaks for the specific tracers of biomass burning (m/z 60 and m/z 73) (Alfarra et
422 al., 2007) than the OOAm, which indicates that the primary BBOA is well represented by this
423 factor. Moreover, the f44 (ratio of m/z 44 (mostly CO_2^+) to total signal in the component mass
424 spectra), an indicator of oxygenated organic species (Alfarra et al., 2007), was higher for the
425 OOAm than for the BBOA_MSY factor, which indicates that this factor corresponds to a more
426 oxidized aerosol. On the other hand, the f43 is higher than the f44 in the BBOA_MSY factor,
427 whereas it is the other way around (f44 much higher than f43) in the OOAm. These differences
428 in relative intensities indicate the differences in the age of the aerosol (Ng et al., 2010) and

433 further lead to differentiate the factors as fresh BBOA and OOAm. The SOA formation from
434 biomass burning has been reported to be quick (Heringa et al., 2011), and hence part of the
435 OOAm factor is formed of aged BBOA, which also explains that the time series of the OOAm
436 factor partially tracks that of the BBOA_MSY. The BBOA_MSY profile found here is very similar
437 to a BBOA profile found for Montseny in March 2009 (Minguillón et al., 2011)
438 (<https://sites.google.com/site/amsglobaldatabase>) and to an average profile for BBOA from
439 various datasets (Ng et al., 2011a) (Figure S9). The f60 in the BBOA_MSY factor is 0.014, similar
440 to the f60 in these other two BBOA profiles (0.017 and 0.024). It has been also compared to
441 the BBOA found in the background of Paris (Crippa et al., 2013), with which some more
442 differences were found, mainly our profile has higher m/z 43 and m/z 41 signals and lower m/z
443 60 (Figure S9). This BBOA_MSY mass spectrum is considered specific for the study area and
444 hence it can be later used for other studies in the region, to be fed to the ME-2 model in order
445 to quantify the BBOA contribution. We have done so in the present study for the winter
446 period. Whereas the time series of both factors were similar, the BBOA_MSY contribution
447 showed more intense peaks, and the increase in the OOAm was slightly higher for the second
448 part of the main peak on the 23 July.

Eliminado: Figure S9

Eliminado: Figure S9

449

450 3.5 Source apportionment of organic aerosol

451 The source apportionment of organic aerosol was carried out separately for the
452 warmer period (14 June to 9 October 2012) and the colder period (28 October 2012 to 7 April
453 2013). The days of the wildfire event were excluded from the warmer period dataset. The
454 separation in two seasons was done to better characterize the source profiles of the different
455 sources, especially the different types of OOA, given that it is expected to vary throughout the
456 year.

457 The application of ME-2 to the warmer period resulted in a solution with 3 factors: a
458 hydrocarbon-like OA (HOA), a semi-volatile oxygenated OA (SV-OOA) and a low-volatile
459 oxygenated OA (LV-OOA). This solution was chosen based on several tests with different
460 number of factors and different α -values for the constrained factors, taking into account the
461 correlations with external data, the diurnal patterns and the residuals, following the strategy
462 described by Crippa et al. (2014) and Canonaco et al. (2013). The HOA factor was constrained
463 using an average HOA factor (HOA_avg) from different datasets (Ng et al., 2011a). An α -value
464 range from 0.05 to 0.3 was explored and an α -value of 0.2 was finally selected, which was a
465 compromise between a higher squared Pearson correlation coefficient between HOA and BC
466 (which increased when increasing the α -value) and the physically meaningful profiles of the

469 whole solution (i.e. assessing the profiles of the LV-OOA and SV-OOA factors). Hence, the a-
470 value 0.05 did not reach converge, and the a-value 0.1 resulted in not-well-resolved OOA
471 factors. BC concentrations correlated moderately with HOA of the chosen solution (squared
472 Pearson coefficient $R^2=0.51$, Table S1). The SV-OOA shows higher 43-to-44 ratio compared to
473 the LV-OOA, together with a lower f44, which are the main differences between these two
474 profiles (Figure 8a). The BBOA contribution in summer is expected to be low based on previous
475 studies carried out in July 2009 (Minguillón et al., 2011) and on the low f60 registered in the
476 present study in summer (Figure S10), which is below the background threshold (0.003)
477 established by Cubison et al. (2011). Hence, the BBOA factor was not identified and it was not
478 constrained by the ME-2 in summer. The correlations of the two OOA factors with external
479 secondary pollutants is not very high (LV-OOA with ammonium shows $R^2=0.43$, LV-OOA with
480 sulphate shows $R^2=0.34$, and SV-OOA with nitrate shows $R^2=0.16$, Table S1). Nevertheless, the
481 source profiles are well defined. The 4-factors solution was investigated and resulted in a split
482 of the LV-OOA factor. The residuals of the 3-factors solution showed an increase between 12h
483 and 15h (which did not disappear in the 4-factors solution), hence indicating the difficulty in
484 explaining the variation of the OA during the middle hours of the day. This pattern was also
485 observed for the m/z 43 variable residuals, whereas it was not observed for other variables.
486 Therefore, the difficulty in the OA explanation may be more related to the SOA formation
487 processes rather than to primary OA sources. Further details on the chosen solution can be
488 found in the supplementary material (Figures S11 to S15).

489 During the warmer period, the HOA accounted for 13% ($0.7 \mu\text{g m}^{-3}$), whereas the LV-
490 OOA and the SV-OOA accounted for 44% and 41% of the total OA ($2.5 \mu\text{g m}^{-3}$ and $2.3 \mu\text{g m}^{-3}$),
491 respectively, hence remaining 2% of unexplained OA mass (Figure 8c). The time series is shown
492 in Figure S16. As explained before, the location and meteorological conditions at MSY result in
493 an increase of pollutants concentrations starting at mid-morning, caused by the breeze
494 transport from populated areas to the regional site. This variation is clearly observed for BC
495 (Figure 9), which showed a moderate correlation with HOA ($R^2=0.51$). Nevertheless, the
496 midday increase in the concentration of SV-OOA is larger than that of BC, and therefore it
497 cannot be only explained by the transport of pollutants, including the SOA formed during the
498 transport, but it is attributed to the formation of SOA during these hours in MSY. Hence, the
499 SOA formation can be estimated as the additional increase with respect to that of BC
500 (considered in % of the average concentration during the night hours), which results in a local
501 SOA formation of $1.1 \mu\text{g m}^{-3}$. This SOA may result mainly from biogenic precursors, in
502 agreement with the 70% of non-fossil SOA found in March 2009 (Minguillón et al., 2011). The
503 flatter diurnal pattern of LV-OOA (Figure 9) points to a more regional and well-oxidized

Eliminado: Figure 8

Eliminado: Figure S10

Eliminado: Figure 8

Eliminado: Figure S16

Eliminado: Figure 9

Eliminado: Figure 9

510 aerosol, which could be interpreted as the regional background SOA. The difference in the
511 diurnal patterns between LV-OOA and SV-OOA is more evident during the regional episodes,
512 evidencing the mixing of the background pollutants (LV-OOA) and the formation of SOA on site
513 (part of the SV-OOA) (Figure S17). This SOA formation during warm periods was also observed
514 by Cusack et al. (2013), who studied nucleation and particle growth events, identifying both of
515 them even under polluted conditions at MSY.

Eliminado: Figure S17

516 In the colder period, the application of ME-2 resulted in a solution with 3 factors:
517 hydrocarbon-like OA (HOA), biomass burning OA (BBOA) and oxygenated OA (OOA) (Figure
518 8b). A solution with two OOA factors was investigated and it was not meaningfully
519 interpretable. Probably the small temperature range variation in winter results in not enough
520 diurnal variation in f43 and f44 for a split of the OOA in SV-OOA and LV-OOA. As per the
521 warmer period, the final solution was chosen based on the strategy described by Crippa et al.
522 (2014) and Canonaco et al. (2013). For coherence with the warmer period, the HOA factor was
523 based in an average HOA factor (HOA_avg) from different datasets (Ng et al., 2011a), and it
524 was constrained with an a-value of 0.1. This a-value was chosen based on the correlation
525 between the HOA contribution and the BC concentrations found for different a-values tests,
526 the source profiles obtained for the rest of the sources (i.e. assuring that they were
527 meaningful), and a preference for relatively low a-values to avoid mixing of OOA sources into
528 the HOA source. The HOA contribution of the chosen solution shows a relatively strong
529 correlation with BC concentrations (squared Pearson coefficient $R^2=0.70$, Table S1). The HOA
530 spectral profiles found for summer and winter are quite similar, and hence the HOA
531 contributions in summer and winter can be compared directly. The BBOA factor was decided
532 to be constrained based on the f60 signal, which was above the aforementioned threshold of
533 0.003 (Figure S10). It was based in the BBOA_MSY profile found for the wildfire episode that

Eliminado: Figure 8

534 took place during this study, constrained with an a-value of 0.1. The a-value was chosen with
535 the following criteria: preference for a low a-value given that the anchor profile used was site-
536 specific, residuals for the m/z 60 not showing any diurnal pattern, contribution of the BBOA
537 factor to the total m/z 60 (which reached 64% for the chosen solution). The resulting BBOA
538 profile has a higher m/z 44 signal than the BBOA_MSY, which may indicate differences in the
539 biomass burning emissions from the wildfire event compared to the emissions from regular
540 biomass burning, or it could indicate that the BBOA contribution identified here may be
541 partially mixed with some oxidized OA. The single winter OOA factor identified shows higher
542 f44 than both LV-OOA and SV-OOA in summer. This higher degree of oxidation of the OA in
543 winter indicates that there is less newly-formed SOA during winter compared to summer. A
544 similar variation was observed in Zurich (Canonaco et al., 2014). The OOA contribution

Eliminado: Figure S10

548 correlates moderately with sulphate ($R^2=0.49$), relatively strongly with nitrate ($R^2=0.73$) and
549 more strongly with ammonium ($R^2=0.79$, Table S1). Further details on the chosen solution can
550 be found in the supplementary material (Figures S11 to S15).

551 The major OA constituent in winter was the OOA, with 59% ($1.5 \mu\text{g m}^{-3}$), whereas the
552 HOA and BBOA accounted for 12% ($0.3 \mu\text{g m}^{-3}$) and 28% ($0.7 \mu\text{g m}^{-3}$) of the total OA,
553 respectively, with only 1% of the OA mass remaining unexplained (Figure 8d). Note that the
554 BBOA contribution may be mixed with some OOA as stated before, given the relatively high
555 signal at m/z 44 and hence the pure BBOA contribution would be lower than that determined.
556 Actually it accounts for 6% of the total signal at m/z 44. Nevertheless, strong correlation
557 ($R^2=0.77$) was found between the BBOA contribution and the potassium concentrations
558 determined in 24-h PM_{10} samples (Figure S18), which further confirms the existence of this
559 source at MSY in winter. The relative BBOA contributions found in the present study are similar
560 to those found in a previous study in March 2009 using a HR-ToF-AMS, where the HOA
561 represented 7% of the total OA, the BBOA contributed with 9% and the rest was attributed to
562 OOA (Minguillón et al., 2011; Crippa et al., 2014). The discrepancy in the BBOA contribution
563 (29% vs 9%) may be due to the different sampling periods (the current study included Nov
564 2012-March 2013 whereas the previous study only included March 2009), to the mixture of
565 some OOA in the BBOA factor for the present study, and/or to the possible increase of biomass
566 burning due to the climate and energy policies in the last five years.

567 The average daily pattern shown by the different OA sources in winter (Figure 9)
568 resembles that of BC, nitrate, sulphate and ammonium (Figure 5), with an increase of
569 pollutants concentrations starting at around 10h UTC and reaching high concentrations at
570 around 13h UTC. No significant differences in the daily pattern were observed for different
571 meteorological episodes, other than the different concentrations (Figure S17). This daily
572 increase is attributed to the transport from populated areas to the mountain site with the
573 breeze. This variation is observed for all the components and therefore the local formation of
574 SOA is deduced to be low in winter.

575

576 4 CONCLUSIONS

577 The deployment of an ACSM at the regional background site of Montseny during one
578 year allowed for the characterization of PM_{10} composition and its variation as a function of time
579 of the year and atmospheric scenarios. The OA sources were also identified and studied.

580 Strong correlation ($R^2=0.66$) was found between total mass determined by ACSM
581 components + BC and PM_{10} determined by an optical particle counter with a slope near to

Eliminado: Figure 8

Eliminado: Figure S18

Eliminado: Figure 9

Eliminado: Figure 5

Eliminado: Figure S17

587 unity. The suitability of the application of a composition-dependent collection efficiency (CE)
588 was confirmed.

589 Strong correlations were found between the ACSM measurements and off-line
590 measurements (filters) for sulphate ($R^2=0.93$), ammonium ($R^2=0.68$) and nitrate ($R^2=0.82$).
591 Nevertheless the slopes differ more than 20% from the unity for nitrate and ammonium.

592 The comparison of the OA measured by the ACSM with the OC measured in filter
593 samples points to a current underestimation of the RIE established for OA.

594 A wildfire episode affected significantly the organic aerosol concentrations. The source
595 profile of fresh BBOA for this specific episode was characterized and it resembles those from
596 other studies. The BBOA contribution in winter correlates with the PM_{10} potassium
597 concentrations.

598 OA was the major component of submicron aerosol on average and especially during
599 the warm periods. Three organic sources were identified by PMF in summer: HOA, SV-OOA
600 and LV-OOA; and three sources in winter: HOA, BBOA and OOA. SOA was the major
601 constituent of the OA at MSY, being more than 80% of total OA in summer and about 60% in
602 winter. The in-situ formation of SOA in summer, happening around midday, was estimated to
603 be $1.1 \mu\text{g m}^{-3}$ on average (20% of OA).

604 Sulphate concentrations were higher in summer, while nitrate concentrations were
605 higher in winter due to environmental conditions (temperature, relative humidity and solar
606 radiation, among others). Sulphate originates from a wider area and is affected by the shipping
607 emissions from the Mediterranean, while the rest of the components may have a nearer
608 origin.

609 As typical for mountain sites, all the pollutants were affected by the general breeze
610 regime, leading to an increase from mid-morning until the afternoon, and a decrease until the
611 evening.

612

613 **ACKNOWLEDGEMENTS**

614 This study was supported by the Spanish Ministry of Economy and Competitiveness
615 and FEDER funds under the project PRISMA (CGL2012-39623-C02-1), by the Generalitat de
616 Catalunya (AGAUR 2014 SGR33 and the DGQA), and by the European Union Seventh
617 Framework Programme (FP7/ 2007-2013) through ACTRIS (grant agreement no 262254). M.C.
618 Minguillón was partially funded by the JAE-Doc CSIC program, co-funded by the European
619 Social Fund (ESF). A. Ripoll was partially funded by a PhD grant from the Spanish Ministry of
620 Economy and Competitiveness through CARIATI (CGL2008-06294/CLI) project.

621

622 **FIGURE CAPTIONS**

623 **Figure 1.** ACSM components + BC concentrations vs PM_{10} measured by the optical counter coloured by
624 the sampling time (dd/mm/yyyy). Line and parameters correspond to least orthogonal distance fit
625 ($y=a+bx$). The wild fire period is excluded from the fit.

626 **Figure 2.** ACSM components concentrations vs 24-h samples concentrations. Lines and parameters
627 correspond to least orthogonal distance fits.

628 **Figure 3.** Time series of ACSM components and BC concentrations during the whole study period.

629 **Figure 4.** Monthly relative chemical composition of submicron aerosol. The numbers on top of each
630 bar represent the average monthly concentration. n is the number of data points for each month
631 (right axis).

632 **Figure 5.** Average daily pattern for (a) the warmer and (b) the colder periods. Note that OA is plotted
633 in the right axis.

634 **Figure 6.** Relative chemical composition of submicron aerosol as a function of the type of scenario.
635 The numbers on top of each bar represent the average concentration for each type of scenario. n is
636 the number of data points for each type of scenario (right axis).

637 **Figure 7.** (a) Time series of ACSM components and BC concentrations and pie chart of the average
638 chemical composition during the wildfire episode from 22nd to 26th July 2012. (b) Time series of the
639 contribution of the BBOA_MSY and Aged BBOA sources identified by PMF. (c) Source profile of the
640 BBOA_MSY and Aged BBOA sources.

641 **Figure 8.** Mass spectral profiles of the organic sources identified for (a) summer and (b) winter.
642 Average contribution of the organic sources to total OA for (c) summer and (d) winter. The white
643 fraction of the pie charts corresponds to unexplained mass.

644 **Figure 9.** Average daily patterns of the organic sources contributions and BC concentrations for (a)
645 summer and (b) winter. Error bars represent standard deviations.

646

647 **SUPPLEMENTARY MATERIAL**

648 **Figure S1.** Frequency of type of scenario for each of the months of the study period.

649 **Figure S2.** Temperature, relative humidity, wind direction and speed, solar radiation and precipitation
650 hourly data at MSY during the study period.

651 **Figure S3.** Time-dependent CE calculated with the Middlebrook approach (Middlebrook et al., 2012).

652 **Figure S4.** ACSM components + BC concentrations vs mass concentration calculated from Scanning
653 Mobility Particle Sizer (SMPS) data coloured by the sampling time (dd/mm/yyyy). Data availability for
654 SMPS data covered only 2012 period. Line and parameters correspond to least orthogonal distance fit
655 ($y=a+bx$). The wild fire period is excluded from the fit.

656 **Figure S5.** Schematic comparison of ACSM components + BC concentrations vs PM_{10} concentrations
657 from OPC corrected with gravimetric determinations. The numbers indicate the slopes found for
658 experimental data for Montseny during June 2012 to July 2013. The 2.25 corresponds to the slope of
659 OA (ACSM) vs OM estimated from OC (filters) as $2*OC$.

660 **Figure S6.** Average daily pattern for (a) Atlantic advections (ATL), (b) North African episodes (NAF), (c)
661 regional episodes (REG), and (d) Winter Anticyclonic episodes (WAE). Note that OA is plotted in the
662 right axis.

663 **Figure S7.** Relative chemical composition as a function of average concentration and number of data
664 points for each range of concentrations. No clear differences are observed.

665 **Figure S8.** Total optical depth, sulphate surface concentration, dust surface concentration, and smoke
666 surface concentration from the NAAPS model for 23, 24 and 25 July 2012 (wildfire event) (a-c), and
667 satellite images from 22 and 23 July 2012 from The Earth Observing System Data and Information
668 System (EOSDIS), NASA's Earth Science Data Systems Program (d, e).

669 **Figure S9.** Comparison of the BBOA factor found for the wildfire episode (BBOA_MSY) with other
670 BBOA profiles found in the literature (Ng et al., 2011a;Crippa et al., 2014).

671 **Figure S10.** Time series of f60 (unitless) and OA concentration ($\mu\text{g m}^{-3}$) throughout the study period at
672 MSY. Dashed line corresponds to the 0.5% threshold for the f60 determined by Cubison et al. (2011).

673 **Figure S11.** Q/Qexp vs number of factors for the warmer and the colder periods. The grey dot in the
674 colder period corresponds to a solution with an a-value of 0.2 for the BBOA factor, given that there
675 was no convergence with an a-value of 0.1 for the 2-factors solution.

676 **Figure S12.** Weighted residuals vs m/z for the warmer and the colder periods.

677 **Figure S13.** Time series of the measured and reconstructed OA concentrations for the warmer and the
678 colder periods.

679 **Figure S14.** Time series of Q/Qexp for the warmer and the colder periods.

680 **Figure S15.** Q/Qexp vs m/z for the warmer and the colder periods.

681 **Figure S16.** Time series of the OA sources in the warmer (top) and the colder (bottom) periods.

682 **Figure S17.** Average daily pattern for Atlantic advections (ATL), for the warmer and the colder periods,
683 regional episodes (REG) (only warmer period), and Winter Anticyclonic episodes (WAE) (only colder
684 period).

685 **Figure S18.** Contribution of BBOA in winter (averaged to 24-h periods matching the filter sampling) vs
686 potassium concentrations in PM_{10} .

687 **Table S1.** Squared Pearson correlation coefficients between OA sources/types and BC, sulphate,
688 nitrate and ammonium for the warmer and the colder periods

689
690

691 REFERENCES

692 Aiken, A. C., Decarlo, P. F., Kroll, J. H., Worsnop, D. R., Huffman, J. A., Docherty, K. S.,
693 Ulbrich, I. M., Mohr, C., Kimmel, J. R., Sueper, D., Sun, Y., Zhang, Q., Trimborn, A., Northway,
694 M., Ziemann, P. J., Canagaratna, M. R., Onasch, T. B., Alfarra, M. R., Prevot, A. S. H., Dommen,
695 J., Duplissy, J., Metzger, A., Baltensperger, U., and Jimenez, J. L.: O/C and OM/OC ratios of
696 primary, secondary, and ambient organic aerosols with high-resolution time-of-flight aerosol
697 mass spectrometry, *Environ. Sci. Technol.*, 42, 4478-4485, 2008.

698 Alastuey, A., Minguillón, M. C., Pérez, N., Querol, X., Viana, M., and de Leeuw, F.: PM10
699 measurement methods and correction factors: 2009 status report, ETC/ACM Technical Paper
700 2011/21, 2011.

701 Alfarra, M. R., Prevot, A. S. H., Szidat, S., Sandradewi, J., Weimer, S., Lanz, V. A.,
702 Schreiber, D., Mohr, M., and Baltensperger, U.: Identification of the mass spectral signature of
703 organic aerosols from wood burning emissions, *Environ. Sci. Technol.*, 41, 5770-5777, 2007.

704 Alves, C., Vicente, A., Pio, C., Kiss, G., Hoffer, A., Decesari, S., Prevôt, A. S. H.,
705 Minguillón, M. C., Querol, X., Hillamo, R., Spindler, G., and Swietlicki, E.: Organic compounds in

706 aerosols from selected European sites - Biogenic versus anthropogenic sources, *Atmos.*
707 *Environ.*, 59, 243-255, 2012.

708 Bougiatioti, A., Stavroulas, I., Kostenidou, E., Zarnpas, P., Theodosi, C., Kouvarakis, G.,
709 Canonaco, F., Prévôt, A. S. H., Nenes, A., Pandis, S. N., and Mihalopoulos, N.: Processing of
710 biomass-burning aerosol in the eastern Mediterranean during summertime, *Atmos. Chem.*
711 *Phys.*, 14, 4793-4807, 2014.

712 Budisulistiorini, S. H., Canagaratna, M. R., Croteau, P. L., Marth, W. J., Baumann, K.,
713 Edgerton, E. S., Shaw, S. L., Knipping, E. M., Worsnop, D. R., Jayne, J. T., Gold, A., and Surratt, J.
714 D.: Real-time continuous characterization of secondary organic aerosol derived from isoprene
715 epoxydiols in downtown Atlanta, Georgia, using the aerodyne aerosol chemical speciation
716 monitor, *Environ. Sci. Technol.*, 47, 5686-5694, 2013.

717 Budisulistiorini, S. H., Canagaratna, M. R., Croteau, P. L., Baumann, K., Edgerton, E. S.,
718 Kollman, M. S., Ng, N. L., Verma, V., Shaw, S. L., Knipping, E. M., Worsnop, D. R., Jayne, J. T.,
719 Weber, R. J., and Surratt, J. D.: Intercomparison of an Aerosol Chemical Speciation Monitor
720 (ACSM) with ambient fine aerosol measurements in downtown Atlanta, Georgia, *Atmos. Meas.*
721 *Tech.*, 7, 1929-1941, 10.5194/amt-7-1929-2014, 2014.

722 Canagaratna, M. R., Jayne, J. T., Jimenez, J. L., Allan, J. D., Alfarra, M. R., Zhang, Q.,
723 Onasch, T. B., Drewnick, F., Coe, H., Middlebrook, A., Delia, A., Williams, L. R., Trimborn, A. M.,
724 Northway, M. J., DeCarlo, P. F., Kolb, C. E., Davidovits, P., and Worsnop, D. R.: Chemical and
725 microphysical characterization of ambient aerosols with the aerodyne aerosol mass
726 spectrometer, *Mass Spectrom. Rev.*, 26, 185-222, 2007.

727 Canonaco, F., Crippa, M., Slowik, J. G., Baltensperger, U., and Prévôt, A. S. H.: SoFi, an
728 IGOR-based interface for the efficient use of the generalized multilinear engine (ME-2) for the
729 source apportionment: ME-2 application to aerosol mass spectrometer data, *Atmospheric*
730 *Measurement Techniques*, 6, 3649-3661, 2013.

731 Canonaco, F., Slowik, J. G., Baltensperger, U., and Prévôt, A. S. H.: Inverse relationship
732 between the degree of oxidation of OOA (oxygenated organic aerosol) and the oxidant OX (O₃
733 +NO₂) due to biogenic emissions, *Atmos. Chem. Phys. Discuss.*, 14, 28079-28104,
734 10.5194/acpd-14-28079-2014, 2014.

735 Carbone, S., Saarikoski, S., Frey, A., Reyes, F., Reyes, P., Castillo, M., Gramsch, E., Oyola,
736 P., Jayne, J., Worsnop, D., and Hillamo, R.: Chemical characterization of submicron Aerosol
737 particles in Santiago de Chile, *Aerosol and Air Quality Research*, 13, 462-473, 2013.

738 Cavalli, F., Viana, M., Yttri, K. E., Genberg, J., and Putaud, J. P.: Toward a standardised
739 thermal-optical protocol for measuring atmospheric organic and elemental carbon: the
740 EUSAAR protocol, *Atmos. Meas. Tech.*, 3, 79-89, 10.5194/amt-3-79-2010, 2010.

741 Crippa, M., DeCarlo, P. F., Slowik, J. G., Mohr, C., Heringa, M. F., Chirico, R., Poulain, L.,
742 Freutel, F., Sciare, J., Cozic, J., Di Marco, C. F., Elsasser, M., Nicolas, J. B., Marchand, N., Abidi,
743 E., Wiedensohler, A., Drewnick, F., Schneider, J., Borrmann, S., Nemitz, E., Zimmermann, R.,
744 Jaffrezo, J. L., Prévôt, A. S. H., and Baltensperger, U.: Wintertime aerosol chemical composition
745 and source apportionment of the organic fraction in the metropolitan area of Paris, *Atmos.*
746 *Chem. Phys.*, 13, 961-981, 10.5194/acp-13-961-2013, 2013.

747 Crippa, M., Canonaco, F., Lanz, V. A., Äijälä, M., Allan, J. D., Carbone, S., Capes, G.,
748 Ceburnis, D., Dall'Osto, M., Day, D. A., DeCarlo, P. F., Ehn, M., Eriksson, A., Freney, E., Ruiz, L.

749 H., Hillamo, R., Jimenez, J. L., Junninen, H., Kiendler-Scharr, A., Kortelainen, A. M., Kulmala, M.,
750 Laaksonen, A., Mensah, A. A., Mohr, C., Nemitz, E., O'Dowd, C., Ovadnevaite, J., Pandis, S. N.,
751 Petäjä, T., Poulain, L., Saarikoski, S., Sellegri, K., Swietlicki, E., Tiitta, P., Worsnop, D. R.,
752 Baltensperger, U., and Prévôt, A. S. H.: Organic aerosol components derived from 25 AMS data
753 sets across Europe using a consistent ME-2 based source apportionment approach, *Atmos.*
754 *Chem. Phys.*, **14**, 6159-6176, 2014.

755 Cubison, M. J., Ortega, A. M., Hayes, P. L., Farmer, D. K., Day, D., Lechner, M. J., Brune,
756 W. H., Apel, E., Diskin, G. S., Fisher, J. A., Fuelberg, H. E., Hecobian, A., Knapp, D. J., Mikoviny,
757 T., Riemer, D., Sachse, G. W., Sessions, W., Weber, R. J., Weinheimer, A. J., Wisthaler, A., and
758 Jimenez, J. L.: Effects of aging on organic aerosol from open biomass burning smoke in aircraft
759 and laboratory studies, *Atmos. Chem. Phys.*, **11**, 12049-12064, 2011.

760 Cusack, M., Alastuey, A., Pérez, N., Pey, J., and Querol, X.: Trends of particulate matter
761 (PM_{2.5}) and chemical composition at a regional background site in the Western
762 Mediterranean over the last nine years (2002–2010), *Atmos. Chem. Phys.*, **12**, 8341-8357,
763 10.5194/acp-12-8341-2012, 2012.

764 Cusack, M., Pérez, N., Pey, J., Wiedensohler, A., Alastuey, A., and Querol, X.: Variability
765 of sub-micrometer particle number size distributions and concentrations in the Western
766 Mediterranean regional background, *Tellus, Series B: Chemical and Physical Meteorology*, **65**,
767 2013.

768 Fröhlich, R., Crenn, V., Setyan, A., Belis, C. A., Canonaco, F., Favez, O., Riffault, V.,
769 Slowik, J. G., Aas, W., Aijälä, M., Alastuey, A., Artiñano, B., Bonnaire, N., Bozzetti, C., Bressi, M.,
770 Carbone, C., Coz, E., Croteau, P. L., Cubison, M. J., Esser-Gietl, J. K., Green, D. C., Gros, V.,
771 Heikkinen, L., Herrmann, H., Jayne, J. T., Lunder, C. R., Minguillón, M. C., Močnik, G., O'Dowd,
772 C. D., Ovadnevaite, J., Petralia, E., Poulain, L., Priestman, M., Ripoll, A., Sarda-Estève, R.,
773 Wiedensohler, A., Baltensperger, U., Sciare, J., and Prévôt, A. S. H.: ACTRIS ACSM
774 intercomparison – Part 2: Intercomparison of ME-2 organic source apportionment results from
775 15 individual, co-located aerosol mass spectrometers, *Atmos. Meas. Tech. Discuss.*, **8**, 1559-
776 1613, 10.5194/amtd-8-1559-2015, 2015.

777 Hawkins, L. N., Russell, L. M., Covert, D. S., Quinn, P. K., and Bates, T. S.: Carboxylic
778 acids, sulfates, and organosulfates in processed continental organic aerosol over the southeast
779 Pacific Ocean during VOCALS-REx 2008, *Journal of Geophysical Research: Atmospheres*, **115**,
780 10.1029/2009jd013276, 2010.

781 Heringa, M. F., DeCarlo, P. F., Chirico, R., Tritscher, T., Dommen, J., Weingartner, E.,
782 Richter, R., Wehrle, G., Prévôt, A. S. H., and Baltensperger, U.: Investigations of primary and
783 secondary particulate matter of different wood combustion appliances with a high-resolution
784 time-of-flight aerosol mass spectrometer, *Atmos. Chem. Phys.*, **11**, 5945-5957, 2011.

785 IPCC: Climate Change 2013: The Physical Science Basis. Contribution of Working Group
786 I to the Fifth Assessment Report of the Intergovernmental Panel on Climate Change, edited by:
787 Stocker, T. F., Qin, D., Plattner, G.-K., Tignor, M., Allen, S. K., Boschung, J., Nauels, A., Xia, Y.,
788 Bex, V., and Midgley, P. M., Cambridge University Press, Cambridge, United Kingdom and New
789 York, NY, USA, 1535 pp pp., 2013.

790 Jimenez, J. L., Canagaratna, M. R., Donahue, N. M., Prevot, A. S. H., Zhang, Q., Kroll, J.
791 H., DeCarlo, P. F., Allan, J. D., Coe, H., Ng, N. L., Aiken, A. C., Docherty, K. S., Ulbrich, I. M.,
792 Grieshop, A. P., Robinson, A. L., Duplissy, J., Smith, J. D., Wilson, K. R., Lanz, V. A., Hueglin, C.,

793 Sun, Y. L., Tian, J., Laaksonen, A., Raatikainen, T., Rautiainen, J., Vaattovaara, P., Ehn, M.,
794 Kulmala, M., Tomlinson, J. M., Collins, D. R., Cubison, M. J., Dunlea, E. J., Huffman, J. A.,
795 Onasch, T. B., Alfarra, M. R., Williams, P. I., Bower, K., Kondo, Y., Schneider, J., Drewnick, F.,
796 Borrmann, S., Weimer, S., Demerjian, K., Salcedo, D., Cottrell, L., Griffin, R., Takami, A.,
797 Miyoshi, T., Hatakeyama, S., Shimono, A., Sun, J. Y., Zhang, Y. M., Dzepina, K., Kimmel, J. R.,
798 Sueper, D., Jayne, J. T., Herndon, S. C., Trimborn, A. M., Williams, L. R., Wood, E. C.,
799 Middlebrook, A. M., Kolb, C. E., Baltensperger, U., and Worsnop, D. R.: Evolution of organic
800 aerosols in the atmosphere, *Science*, 326, 1525-1529, 2009.

801 Liu, P. S. K., Deng, R., Smith, K. A., Williams, L. R., Jayne, J. T., Canagaratna, M. R.,
802 Moore, K., Onasch, T. B., Worsnop, D. R., and Deshler, T.: Transmission efficiency of an
803 aerodynamic focusing lens system: Comparison of model calculations and laboratory
804 measurements for the aerodyne aerosol mass spectrometer, *Aerosol Sci. Technol.*, 41, 721-
805 733, 2007.

806 Middlebrook, A. M., Bahreini, R., Jimenez, J. L., and Canagaratna, M. R.: Evaluation of
807 composition-dependent collection efficiencies for the Aerodyne aerosol mass spectrometer
808 using field data, *Aerosol Sci. Technol.*, 46, 258-271, 2012.

809 Millán, M. M., Salvador, R., Mantilla, E., and Kallos, G.: Photooxidant dynamics in the
810 Mediterranean basin in summer: Results from European research projects, *Journal of*
811 *Geophysical Research D: Atmospheres*, 102, 8811-8823, 1997.

812 Minguillón, M. C., Perron, N., Querol, X., Szidat, S., Fahrni, S. M., Alastuey, A., Jimenez,
813 J. L., Mohr, C., Ortega, A. M., Day, D. A., Lanz, V. A., Wacker, L., Reche, C., Cusack, M., Amato,
814 F., Kiss, G., Hoffer, A., Decesari, S., Moretti, F., Hillamo, R., Teinilä, K., Seco, R., Peñuelas, J.,
815 Metzger, A., Schallhart, S., Müller, M., Hansel, A., Burkhardt, J. F., Baltensperger, U., and Prévôt,
816 A. S. H.: Fossil versus contemporary sources of fine elemental and organic carbonaceous
817 particulate matter during the DAURE campaign in Northeast Spain, *Atmos. Chem. Phys.*, 11,
818 12067-12084, 10.5194/acp-11-12067-2011, 2011.

819 Ng, N. L., Canagaratna, M. R., Zhang, Q., Jimenez, J. L., Tian, J., Ulbrich, I. M., Kroll, J. H.,
820 Docherty, K. S., Chhabra, P. S., Bahreini, R., Murphy, S. M., Seinfeld, J. H., Hildebrandt, L.,
821 Donahue, N. M., DeCarlo, P. F., Lanz, V. A., Prévôt, A. S. H., Dinar, E., Rudich, Y., and Worsnop,
822 D. R.: Organic aerosol components observed in Northern Hemispheric datasets from Aerosol
823 Mass Spectrometry, *Atmos. Chem. Phys.*, 10, 4625-4641, 10.5194/acp-10-4625-2010, 2010.

824 Ng, N. L., Canagaratna, M. R., Jimenez, J. L., Zhang, Q., Ulbrich, I. M., and Worsnop, D.
825 R.: Real-time methods for estimating organic component mass concentrations from aerosol
826 mass spectrometer data, *Environ. Sci. Technol.*, 45, 910-916, 2011a.

827 Ng, N. L., Herndon, S. C., Trimborn, A., Canagaratna, M. R., Croteau, P. L., Onasch, T. B.,
828 Sueper, D., Worsnop, D. R., Zhang, Q., Sun, Y. L., and Jayne, J. T.: An Aerosol Chemical
829 Speciation Monitor (ACSM) for routine monitoring of the composition and mass
830 concentrations of ambient aerosol, *Aerosol Sci. Technol.*, 45, 770-784, 2011b.

831 Paatero, P., and Tapper, U.: Positive matrix factorization: a non-negative factor model
832 with optimal utilization of error estimates of data values, *Environmetrics*, 5, 111-126, 1994.

833 Paatero, P.: The multilinear engine - a table-driven, least squares program for solving
834 multilinear problems, including the n-way parallel factor analysis model, *Journal of*
835 *Computational and Graphical Statistics*, 8, 854-888, 1999.

836 Pérez, N., Pey, J., Castillo, S., Viana, M., Alastuey, A., and Querol, X.: Interpretation of
837 the variability of levels of regional background aerosols in the Western Mediterranean, *Sci.*
838 *Total Environ.*, 407, 527-540, 2008.

839 Petit, J. E., Favez, O., Sciare, J., Crenn, V., Sarda-Estève, R., Bonnaire, N., Močnik, G.,
840 Dupont, J. C., Haeffelin, M., and Leoz-Garziandia, E.: Two years of near real-time chemical
841 composition of submicron aerosols in the region of Paris using an Aerosol Chemical Speciation
842 Monitor (ACSm) and a multi-wavelength Aethalometer, *Atmos. Chem. Phys. Discuss.*, 14,
843 24221-24271, 10.5194/acpd-14-24221-2014, 2014.

844 Petzold, A., Ogren, J. A., Fiebig, M., Laj, P., Li, S. M., Baltensperger, U., Holzer-Popp, T.,
845 Kinne, S., Pappalardo, G., Sugimoto, N., Wehrli, C., Wiedensohler, A., and Zhang, X. Y.:
846 Recommendations for reporting black carbon measurements, *Atmos. Chem. Phys.*, 13, 8365-
847 8379, 2013.

848 Pey, J., Pérez, N., Castillo, S., Viana, M., Moreno, T., Pandolfi, M., López-Sebastián, J.
849 M., Alastuey, A., and Querol, X.: Geochemistry of regional background aerosols in the Western
850 Mediterranean, *Atmospheric Research*, 94, 422-435, 2009.

851 Pey, J., Pérez, N., Querol, X., Alastuey, A., Cusack, M., and Reche, C.: Intense winter
852 atmospheric pollution episodes affecting the Western Mediterranean, *Sci. Total Environ.*, 408,
853 1951-1959, 2010.

854 Pope III, C. A., and Dockery, D. W.: Health effects of fine particulate air pollution: Lines
855 that connect, *Journal of the Air and Waste Management Association*, 56, 709-742, 2006.

856 Querol, X., Alastuey, A., Pey, J., Cusack, M., Pérez, N., Mihalopoulos, N., Theodosi, C.,
857 Gerasopoulos, E., Kubilay, N., and Koçak, M.: Variability in regional background aerosols within
858 the Mediterranean, *Atmos. Chem. Phys.*, 9, 4575-4591, 2009.

859 Querol, X., Alastuey, A., Viana, M., Moreno, T., Reche, C., Minguillón, M. C., Ripoll, A.,
860 Pandolfi, M., Amato, F., Karanasiou, A., Pérez, N., Pey, J., Cusack, M., Vázquez, R., Plana, F.,
861 Dall'Osto, M., De La Rosa, J., Sánchez De La Campa, A., Fernández-Camacho, R., Rodríguez, S.,
862 Pio, C., Alados-Arboledas, L., Titos, G., Artiñano, B., Salvador, P., García Dos Santos, S., and
863 Fernández Patier, R.: Variability of carbonaceous aerosols in remote, rural, urban and industrial
864 environments in Spain: Implications for air quality policy, *Atmos. Chem. Phys.*, 13, 6185-6206,
865 2013.

866 Querol, X., Alastuey, A., Pandolfi, M., Reche, C., Pérez, N., Minguillón, M. C., Moreno,
867 T., Viana, M., Escudero, M., Orío, A., Pallarés, M., and Reina, F.: 2001-2012 trends on air quality
868 in Spain, *Sci. Total Environ.*, 490, 957-969, 2014.

869 Ripoll, A., Minguillón, M. C., Pey, J., Jimenez, J. L., Day, D. A., Querol, X., and Alastuey,
870 A.: Long-term real-time chemical characterization of submicron aerosols at Montsec (Southern
871 Pyrenees, 1570 m a.s.l.), *Atmos. Chem. Phys. Discuss.*, 14, 28809-28844, 10.5194/acpd-14-
872 28809-2014, 2014a.

873 Ripoll, A., Minguillón, M. C., Pey, J., Pérez, N., Querol, X., and Alastuey, A.: Joint
874 analysis of continental and regional background environments in the Western Mediterranean:
875 PM₁ and PM₁₀ concentrations and composition, *Atmos. Chem. Phys. Discuss.*, 14, 16001-
876 16041, 10.5194/acpd-14-16001-2014, 2014b.

877 Shaw, S. L., Baumann, K., Budisulistiorini, S., Canagaratna, M., Croteau, P., Edgerton, E.,
878 Jansen, J., Jayne, J., Knipping, E., Marth, W., Mueller, S., Ng, S., Surratt, J., Tanner, R., and
879 Weber, R.: Operation of the aerosol chemical speciation monitor (ACSM) in the southeastern
880 U.S, 2012, 110-114,

881 Sun, Y., Wang, Z., Dong, H., Yang, T., Li, J., Pan, X., Chen, P., and Jayne, J. T.:
882 Characterization of summer organic and inorganic aerosols in Beijing, China with an Aerosol
883 Chemical Speciation Monitor, *Atmos. Environ.*, 51, 250-259, 2012.

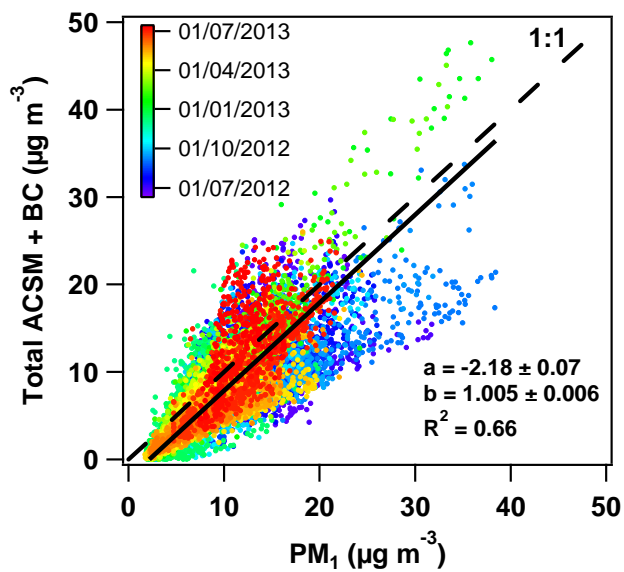
884 Sun, Y., Wang, Z., Fu, P., Jiang, Q., Yang, T., Li, J., and Ge, X.: The impact of relative
885 humidity on aerosol composition and evolution processes during wintertime in Beijing, China,
886 *Atmos. Environ.*, 77, 927-934, 2013a.

887 Sun, Y. L., Wang, Z. F., Fu, P. Q., Yang, T., Jiang, Q., Dong, H. B., Li, J., and Jia, J. J.:
888 Aerosol composition, sources and processes during wintertime in Beijing, China, *Atmos. Chem.*
889 *Phys.*, 13, 4577-4592, 2013b.

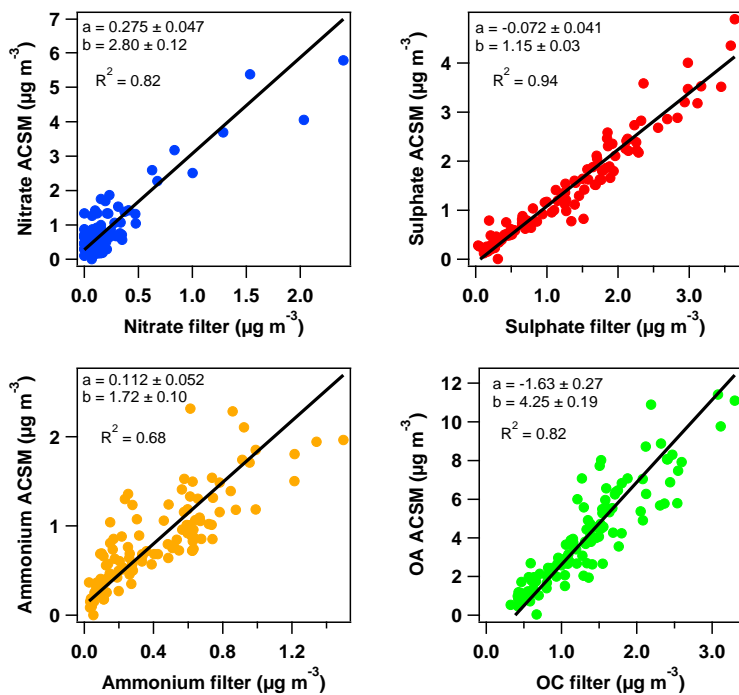
890 Takahama, S., Johnson, A., Guzman Morales, J., Russell, L. M., Duran, R., Rodriguez, G.,
891 Zheng, J., Zhang, R., Toom-Saunty, D., and Leatch, W. R.: Submicron organic aerosol in
892 Tijuana, Mexico, from local and Southern California sources during the CalMex campaign,
893 *Atmos. Environ.*, 70, 500-512, 2013.

894 Van Drooge, B. L., Cusack, M., Reche, C., Mohr, C., Alastuey, A., Querol, X., Prevot, A. S.
895 H., Day, D. A., Jimenez, J. L., and Grimalt, J. O.: Molecular marker characterization of the
896 organic composition of submicron aerosols from Mediterranean urban and rural environments
897 under contrasting meteorological conditions, *Atmos. Environ.*, 61, 482-489, 2012.

898 Wiedensohler, A., Birmili, W., Nowak, A., Sonntag, A., Weinhold, K., Merkel, M.,
899 Wehner, B., Tuch, T., Pfeifer, S., Fiebig, M., Fjåraa, A. M., Asmi, E., Sellegri, K., Depuy, R.,
900 Venzac, H., Villani, P., Laj, P., Aalto, P., Ogren, J. A., Swietlicki, E., Williams, P., Roldin, P.,
901 Quincey, P., Hüglin, C., Fierz-Schmidhauser, R., Gysel, M., Weingartner, E., Riccobono, F.,
902 Santos, S., Grüning, C., Faloon, K., Beddows, D., Harrison, R., Monahan, C., Jennings, S. G.,
903 O'Dowd, C. D., Marinoni, A., Horn, H. G., Keck, L., Jiang, J., Scheckman, J., McMurry, P. H.,
904 Deng, Z., Zhao, C. S., Moerman, M., Henzing, B., De Leeuw, G., Löschau, G., and Bastian, S.:
905 Mobility particle size spectrometers: Harmonization of technical standards and data structure
906 to facilitate high quality long-term observations of atmospheric particle number size
907 distributions, *Atmospheric Measurement Techniques*, 5, 657-685, 2012.
908
909
910

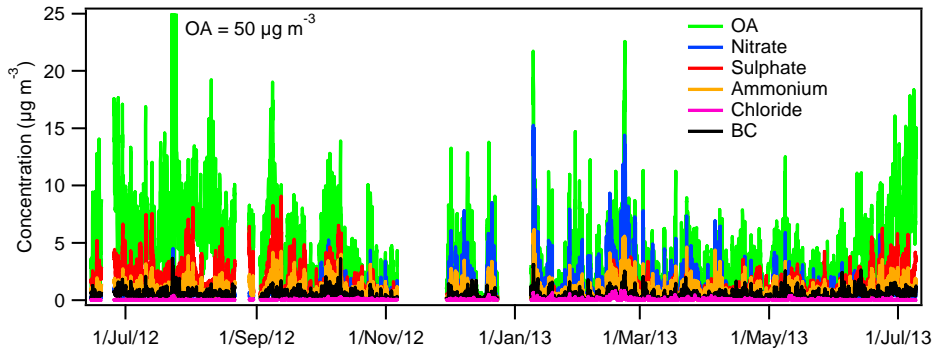


911
 912 **Figure 1**
 913
 914



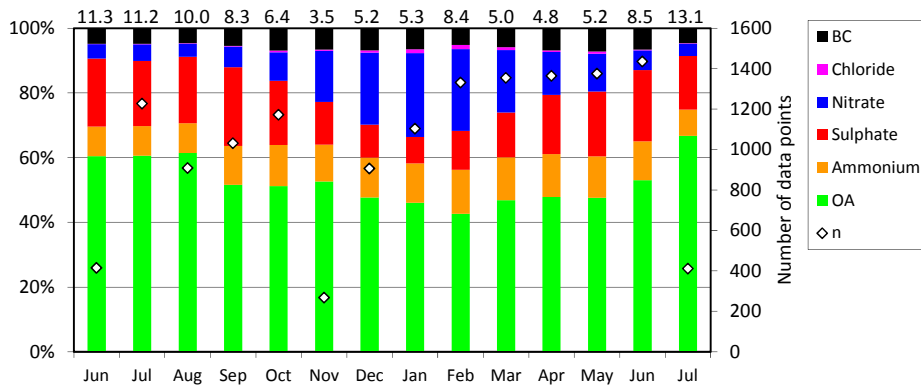
915
 916
 917
 918 **Figure 2**

919
920



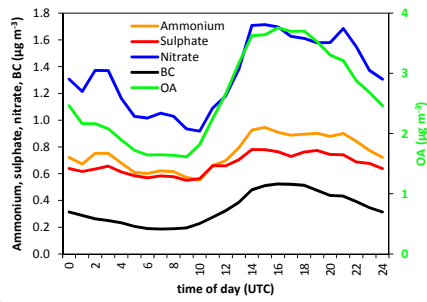
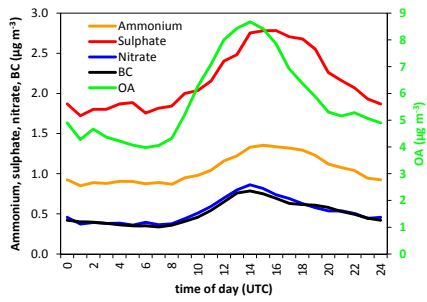
921
922
923
924
925

Figure 3



926
927
928
929
930
931

Figure 4



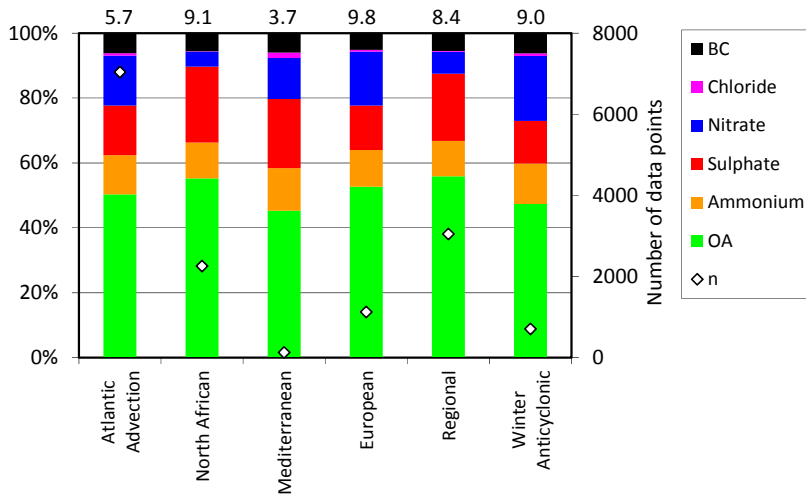
932 a)

b)

933 **Figure 5**

934

935



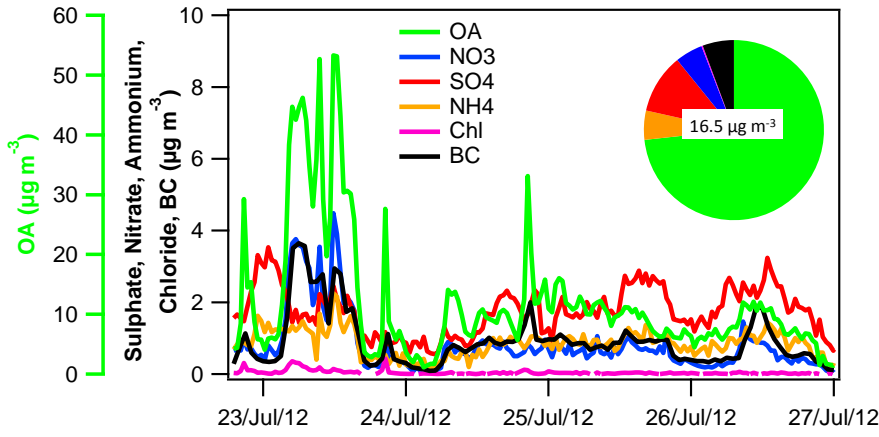
936

937 **Figure 6**

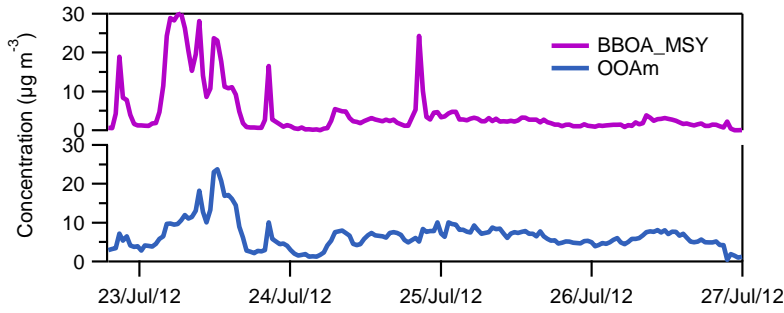
938

939

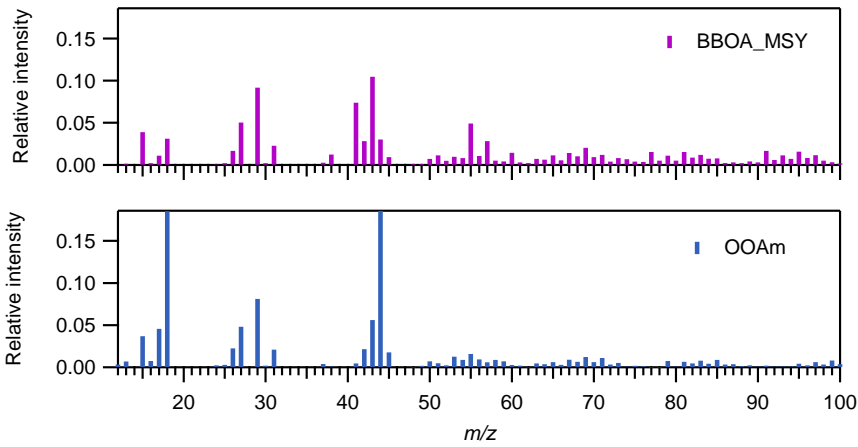
940



941 a)



942 b)



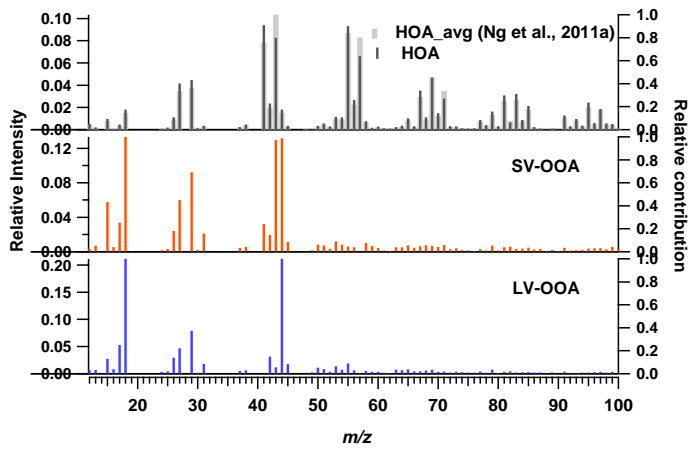
943

944 c)

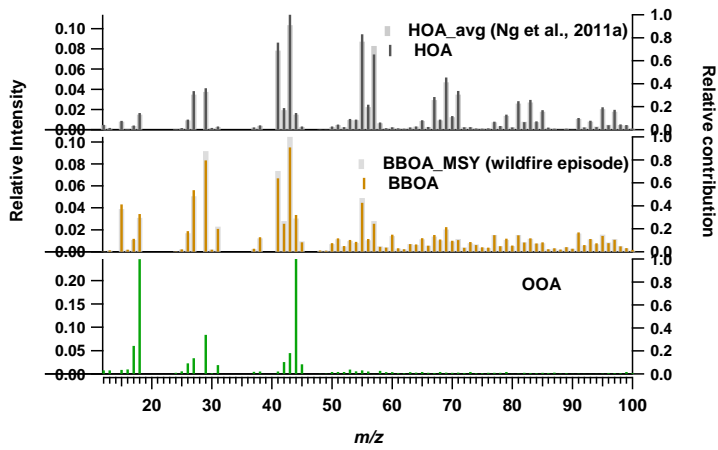
945 **Figure 7**

946

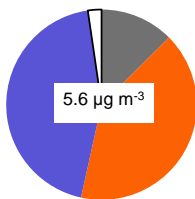
947



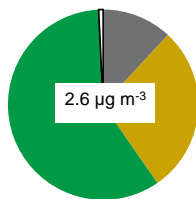
948 a)



949 b)



950 c)



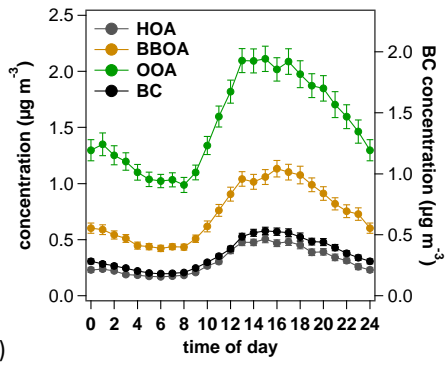
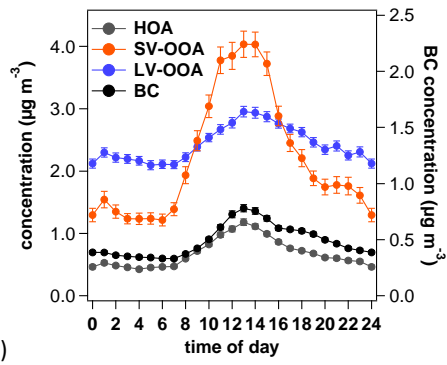
951 d)

952

952 **Figure 8**

953

954



955 a)

b)

956

957 **Figure 9**

958

959